Dissociative Host-Dopant Bonding Facilitates Molecular Doping in Halide Perovskites

Luis Lanzetta,[1] Luca Gregori,[2,3] Luis Huerta Hernandez,[1] Anirudh Sharma,[1] Stefanie Kern,[4] Anna M. Kotowska,[4] Abdul-Hamid Emwas,[5] Luis Gutiérrez-Arzaluz,[6] David J. Scurr,[4] Matthew Piggott,[4] Daniele Meggiolaro,[2] Md Azimul Haque,[1] Filippo De Angelis,[2,3,7,8] Derya Baran[1]**

[1]King Abdullah University of Science and Technology (KAUST), Physical Science and Engineering Division (PSE), KAUST Solar Center (KSC), Thuwal, 23955-6900, Saudi Arabia.

[2]Computational Laboratory for Hybrid/Organic Photovoltaics (CLHYO), Istituto CNR di Scienze e Tecnologie Chimiche "'Giulio Natta"' (CNR-SCITEC), Via Elce di Sotto 8, 06123 Perugia, Italy.

[3]Department of Chemistry, Biology and Biotechnology, University of Perugia, Via Elce di Sotto 8, 06123, Perugia, Italy.

[4]Advanced Materials and Healthcare Technologies, School of Pharmacy, University of Nottingham, Nottingham, NG7 2RD, UK.

[5]King Abdullah University of Science and Technology (KAUST), Core Labs, Thuwal 23955-6900, Saudi Arabia.

[6]King Abdullah University of Science and Technology (KAUST), Physical Science and Engineering Division (PSE), Advanced Membranes and Porous Materials and Catalysis Center, Thuwal 23955, Saudi Arabia.

[7]Department of Mechanical Engineering, College of Engineering, Prince Mohammad Bin Fahd University, P.O. Box 1664, Al Khobar, 31952, Saudi Arabia.

[8]SKKU Institute of Energy Science and Technology (SIEST) Sungkyunkwan University, Suwon, Korea 440-746.

Corresponding Authors

*Daniele Meggiolaro; email: daniele.meggiolaro@cnr.it

*Derya Baran; email: derya.baran@kaust.edu.sa

ABSTRACT

Molecular doping is a promising strategy to fine-tune the electronic properties of halide perovskites and accelerate their implementation as next-generation optoelectronics. However, a deeper understanding of the role of host-dopant interactions in these systems is needed to fully exploit the potential of this avenue. Herein, we demonstrate a surface post-treatment strategy employing n-type molecular dopant n-DMBI-H to modulate free hole density in p-type $CH_3NH_3Sn_{0.75}Pb_{0.25}I_3$ films. We show that the adsorption of n-DMBI-H on surface Sn atoms, followed by the dissociation of an electron-donating hydride from the dopant, facilitates charge transfer to perovskite and hole trapping at the dissociated hydride. We identify this mechanism as a key factor dictating doping compensation in perovskite, allowing carrier density control within nearly one order of magnitude via the dissociated molecular dopant located at film surfaces and grain boundaries. We then exploit n-DMBI-H in perovskite/transport layer junctions, achieving reduced carrier losses and improved contact selectivity and performance in p-i-n, Sn-rich perovskite solar cells. We expect this work to provide carrier density tuning guidelines for a broad range of tin-based perovskite applications.

TOC GRAPHICS

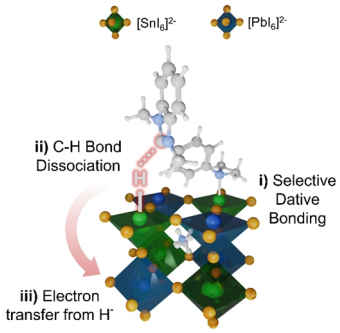

Halide perovskites have become front-runners for next-generation optoelectronics, showcasing a high absorption coefficient, defect tolerance and photovoltaic efficiencies over 25%.[1–3] To enable further breakthroughs in existing applications and meet the needs of a broader range of technologies, it is essential to carefully control their electronic properties. Electronic doping allows the modulation of carrier density using defects and/or additives, becoming crucial towards optimal perovskite energetics and charge transport.[4,5] This allows to obtain high-quality junctions in solar cells and light-emitting diodes (LEDs),[6] to engineer high-performance p- and n-type transistors,[7,8] and to enhance the photocatalytic properties of this class of materials.[9]

Although perovskites can be electronically modified through various methods (e.g., substitutional/interstitial doping or native defect doping/self-doping),[10,11] this remains challenging since typical strategies can introduce energetic disorder. Substitutional Bi^{3+} salts are known to generate mid-bandgap states that cause lower carrier lifetime and mobility.[12] Likewise, vacancy modulation additives (e.g., SnF_2) employed to manipulate self-doping in Sn perovskite may form secondary phases that favor non-radiative recombination.[13] Alternatively, molecular doping constitutes a promising avenue to transfer/extract charges to/from perovskite without compromising its crystal structure.[4,5] However, this route remains largely unexplored in

perovskites, where it has mostly been used to optimize electrical conductivity and band alignment in solar cells.[6,14–16]

In particular, n-type molecular dopants have been elusive vs. their p-type counterparts due to their higher ambient sensitivity. Amongst them, (4-(1,3-dimethyl-2,3-dihydro-1H-benzoimidazol-2-yl)phenyl)-N,N-dimethylbenzenamine (n-DMBI-H) and its derivatives stand out for being air-stable and yielding strong doping in organic semiconductors, where they are regarded as state-of-the-art molecular dopants.[17,18] Their doping mechanism (typically reported as the thermally-assisted cleavage of a carbon-labile hydrogen bond to form a strong electron-donating species, i.e., a molecular radical or a hydride)[19] also makes this class of molecules attractive to induce favorable charge transfer in a broad range of hosts. Chen et al. and Huang et al. employed thiophene- and diphenylaniline-based n-DMBI-H analogues, respectively, to enhance interfacial electronic contact in Pb perovskite solar cells.[20,21] However, the physicochemical processes governing molecular doping in perovskite/n-DMBI-H systems remain unknown. Critically, the key atomic-scale perovskite-dopant interactions dictating the underlying doping mechanism must be clarified to establish rational guidelines for charge carrier density modulation. This is important in molecular dopants containing Lewis base moieties (e.g., amino and/or imidazole groups in n-DMBI-H) that may coordinate with perovskite metallic ions, deeply influencing charge transfer reactions, defect passivation and the overall electronic landscape of the material.

Lower-toxicity, p-type Sn-based perovskites rely on doping compensation (i.e., lowering their high free hole density by introducing electron donors) for their technological deployment.[22] This is crucial to mitigate fast non-radiative recombination in solar cells and LEDs,[23,24] and would greatly benefit emerging applications such as Sn perovskite transistors (which require moderate hole densities for suitable channel conduction)[25] and all-perovskite thermoelectric generators (where n-

type Sn perovskite are highly sought-after).[5] The use of n-type molecular dopants on Sn-based perovskites represents a potential path towards this goal,[26] yet it has been underexplored to date.

Combining i) electrical, spectroscopy and imaging techniques and ii) ab initio simulations, we elucidate the doping compensation mechanism in p-type $CH_3NH_3Sn_{0.75}Pb_{0.25}I_3$ ($MASn_{0.75}Pb_{0.25}I_3$) perovskite thin films employing n-DMBI-H as a post-treatment n-type molecular dopant. We identify selective dative bonding between n-DMBI-H amino groups and perovskite surface Sn sites as a key interaction that enables dopant-to-perovskite charge transfer through dissociation of a C-H bond (Scheme 1). We show that this mechanism dictates doping compensation in perovskite, reducing free hole density by nearly one order of magnitude via n-DMBI-H located at film surfaces and grain boundaries. Finally, we exploit this avenue in perovskite/PCBM junctions, mitigating self-doping-related carrier losses and improving contact selectivity and performance in p-i-n, Sn-rich perovskite solar cells. We expect these findings to enable effective molecular doping guidelines, paving the way towards future perovskite-based technologies.

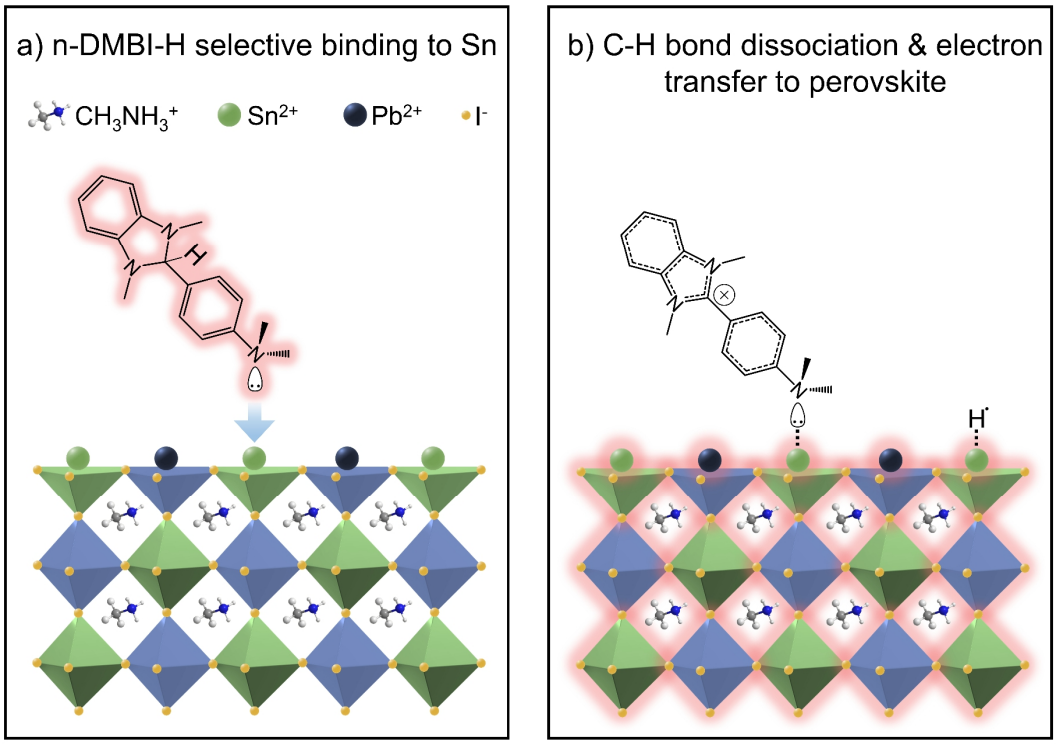

Scheme 1. Doping compensation mechanism of n-DMBI-H in Sn-rich perovskite ($MASn_{0.75}Pb_{0.25}I_3$ in this work). N-DMBI-H selectively attaches to perovskite Sn surface sites via dative bonding (**a**), followed by the dissociation of the C-labile hydrogen bond in n-DMBI-H and dopant-to-perovskite electron transfer (i.e., perovskite hole trapping at dissociated hydride) (**b**).

$MASn_{0.75}Pb_{0.25}I_3$ films were prepared as described in the Experimental Section (Supporting Information). A Sn-rich perovskite composition with a small portion of Pb was chosen to i) yield higher electronic stability than Sn-only analogues[27] and ii) compare the effect of the two metals on potential host-dopant interactions. To preserve sample morphology and specifically assess the effect of n-DMBI-H, the molecular dopant was applied onto fully processed perovskite films as a post-treatment solution (0.01, 0.11, 1.12 and 11.22 mM). X-ray diffraction (XRD) reveals highly crystalline perovskite films with tetragonal structure and preferential orientation in the [h00] direction (Figure S1).[1] Perovskite diffraction patterns remain unchanged upon addition of n-

DMBI-H, confirming that the molecular dopant does not alter the perovskite crystal structure or its lattice parameters.

To detect possible perovskite-dopant interactions (i.e., dative bonding) between n-DMBI-H Lewis base moieties (i.e., imidazole, amino) and $MASn_{0.75}Pb_{0.25}I_3$ Lewis acid sites (e.g., Sn^{2+}, Sn^{4+}, Pb^{2+}), we analyze changes in chemical environment upon n-DMBI-H treatment at samples surfaces via X-ray Photoelectron Spectroscopy (XPS; surface sensitivity: <5 nm). Figure 1a shows Sn $3d_{5/2}$ peaks of control and n-DMBI-H-treated perovskite (0 mM and 1.12 mM, respectively) deconvoluted into two components, assigned to i) perovskite Sn^{2+} ions and ii) Sn^{4+} states typically detected at perovskite surfaces.[28] The origins of the smaller Sn^{2+}-to-Sn^{4+} ratio in the n-DMBI-H-treated film (Table S1) are discussed in Supplementary Note 1. We observe a binding energy decrease for both Sn^{2+} and Sn^{4+} components (~0.1 and ~0.2 eV, respectively) in the n-DMBI-H-treated film vs the bare perovskite sample. This is consistent with higher electron density in Sn sites upon molecular dopant adsorption[29,30] and suggests both Sn^{2+} and Sn^{4+} act as anchoring points for n-DMBI-H, being their Lewis acidity a key factor governing perovskite-dopant interactions. Indeed, Sn^{4+} shows a larger chemical shift next to Sn^{2+} due to its more acidic character, while Pb 4f signals assigned to Pb^{2+} sites show no apparent shift (Figure S4), being the weakest Lewis acid ($Sn^{4+} > Sn^{2+} > Pb^{2+}$). We therefore conclude that n-DMBI-H binds to perovskite surfaces via selective dative bond formation with Sn states.

We further focus on the N 1s XPS signals of Lewis base moieties in n-DMBI-H. For this, we compare a reference n-DMBI-H film with control (0 mM) and n-DMBI-H-treated (1.12 mM) perovskite samples (Figure 1b). The signal of reference n-DMBI-H is deconvoluted into two components, i.e., pristine n-DMBI-H (~399.9 eV) and oxidized n-DMBI-H (~401.5 eV)[31,32] (further details provided in Supplementary Note 2). In control perovskite (0 mM), a single

component assigned to MA^+ cations is detected (~402.2 eV).[28] It is apparent that the contribution of oxidized n-DMBI-H is stronger in the n-DMBI-H-treated perovskite film (1.12 mM) vs the pristine n-DMBI-H sample (66% vs 26%, respectively; Table S1). This is consistent with electron donation from the molecular dopant to perovskite. To validate the perovskite-dopant interaction observed previously, we compare the chemical shifts of N 1s components across all samples in Figure 1b; in this case, we expect molecular dopant signals to shift towards higher binding energies due to electron density loss around N upon dative bond formation.[29,30] Interestingly, we only observe a binding energy increase (~0.2 eV) in the oxidized n-DMBI-H peak of n-DMBI-H-treated perovskite film with respect to the bare molecular dopant sample (labeled as 1.12 mM and n-DMBI-H in Figure 1b, respectively). This indicates that n-DMBI-H bonded to perovskite surface is oxidized, suggesting that only those dopant molecules that undergo Lewis acid-base interactions with the perovskite proceed to transfer their charge to the host. These results identify host-dopant dative bonding as a key step to enable charge transfer.

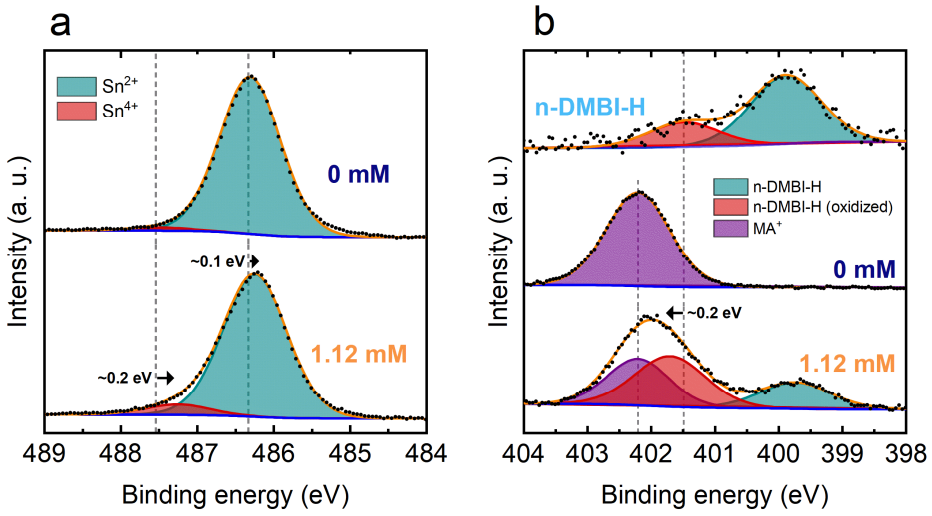

Figure 1. a. Sn $3d_{5/2}$ XPS spectra of control (0 mM) and n-DMBI-H-treated (1.12 mM) perovskite films. Dashed lines: positions of Sn^{2+} and Sn^{4+} components in control perovskite sample. **b.** N *1s* XPS spectra of an n-DMBI-H film (n-DMBI-H) and control and n-DMBI-H-treated perovskite

films (0 mM and 1.12 mM, respectively). Dashed lines: positions of the oxidized n-DMBI-H component in the n-DMBI-H sample and the MA^+ component in the perovskite control sample.

We employ density functional theory (DFT) simulations to examine the bond between n-DMBI-H and the perovskite and to elucidate possible charge transfer mechanisms. For this, we investigate the interaction of an n-DMBI-H molecule with the $Sn_{0.5}Pb_{0.5}I_2$-terminated (001) surface of a reference $MASn_{0.5}Pb_{0.5}I_3$ system, as specified in the Computational Details (Supporting Information). We analyze n-DMBI-H adsorption considering two alternative binding groups in the molecule, i.e., amino group vs imidazole ring, and find the former to yield the most stable perovskite-dopant interaction (Figure S5). n-DMBI-H adsorption through the amino group is calculated ~0.4 eV more favorable at the Sn site relative to Pb (Table S2), in accordance with our experimental observations.

We next explore the possible charge transfer pathways that can lead to perovskite doping compensation following molecular adsorption. As tin-halide perovskites are inherently p-doped by the presence of Sn vacancies,[11] we investigated the charge transfer process by calculating the trapping energy of the hole on the adsorbed molecule at the surface, thus simulating the molecule@perovskite system in the neutral state and in presence of one positive charge. The analysis has been extended to include the possible temperature-activated cleavage of the C-H bond between the imidazole ring and its labile proton at the surface (see Reactions 1 and 2 and Table S3).

(n-DMBI-H)@ Perovskite → (n-DMBI$^+$ + H$^-$)@Perovskite, ΔE = +0.43 eV (1)

+h$^+$ ↓ ΔE = -0.77 eV +h$^+$ ↓ ΔE = -0.99 eV

(n-DMBI-H)$^+$@ Perovskite → (n-DMBI$^+$ + H$^•$)@Perovskite, ΔE = +0.21eV (2)

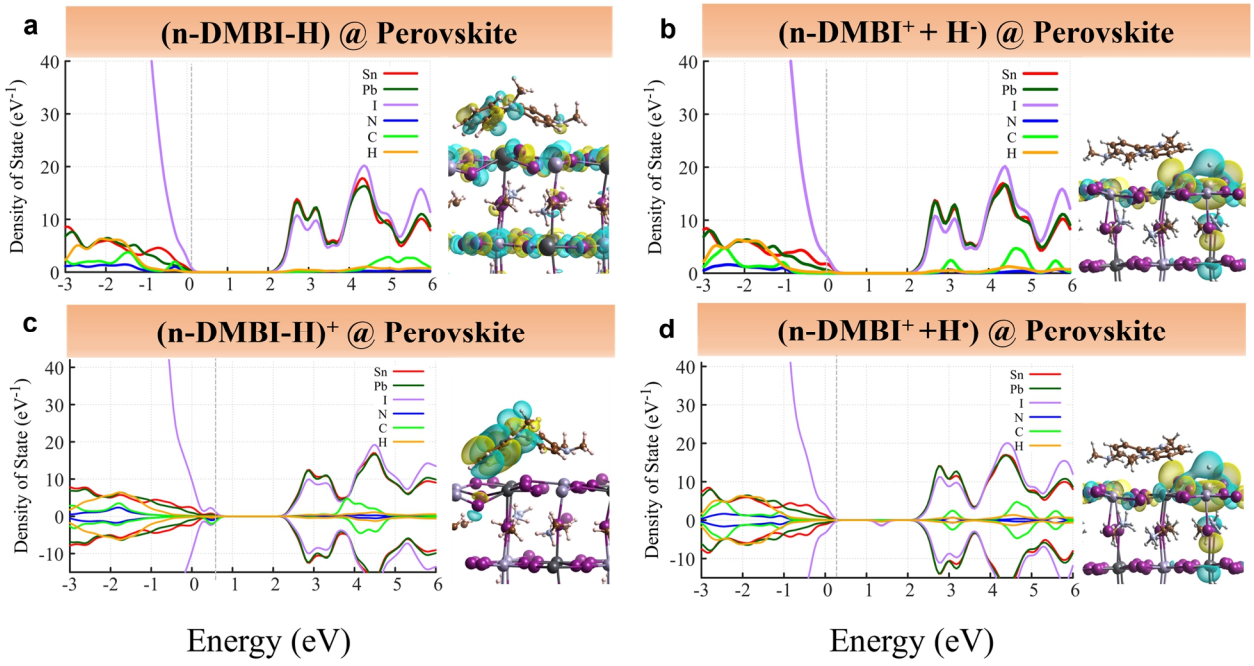

Figure 2. pDOS and frontier orbital plots of **a.** (n-DMBI-H)@ Perovskite; **b.** (n-DMBI$^+$ + H$^-$)@Perovskite; **c.** (n-DMBI-H)$^+$@ Perovskite; **d.** (n-DMBI$^+$ + H$^•$)@Perovskite, calculated at PBE0 level of theory. For **a.** and **b.**, the highest occupied molecular orbital (HOMO) is plotted, while for positively charged systems the lowest unoccupied orbital (LUMO). Dashed lines in the pDOS diagrams indicate the energy of the highest occupied states.

Both the homolytic and heterolytic n-DMBI-H$_{(ads)}$ surface dissociation were investigated in the neutral case. In the homolytic bond cleavage, the n-DMBI-H molecule dissociates into a n-DMBI$^•_{(ads)}$ molecular radical species[19,33] and a radical hydrogen H$^•_{(ads)}$, while for the heterolytic cleavage, the molecule provides two ionic species, i.e. n-DMBI$^+_{(ads)}$ and a hydride, H$^-$. DFT

analysis shows that the dissociation of the neutral n-DMBI-H molecule at the surface is thermodynamically unfavorable by 1.57 and 0.43 eV in the homo- and hetero- bond cleavage cases, respectively (see Table S3), indicating that the heterolytic dissociation is the most probable temperature-activated dissociation path in the neutral state (Reaction 1).

The projected density of states (pDOS) of the n-DMBI-H@Perovskite and the (n-$DMBI^+$ + H^-)@Perovskite systems are reported in Figure 2a and 2b. For the sake of comparison, the pDOS of $MASn_{0.5}Pb_{0.5}I_3$ reference system and additional perovskite-dopant systems are presented in Figure S6 and S7, respectively. In the case of n-DMBI-H@Perovskite, we observe a new state (N, C, H) near the valence band maximum (VBM) of the perovskite system assigned to the HOMO of the adsorbed n-DMBI-H molecule. Correspondingly, the charge density isosurface plot of the last occupied state reveals a clear charge localization on the molecule. Similarly, in the (n-$DMBI^+$ + H^-)@Perovskite system a new state emerges near the VBM, but it is associated with the negative H adsorbed at the surface (see Figure 2b).

These results indicate that charge transfer between a perovskite VBM hole and the localized states introduced by the molecule dopant are responsible for the de-doping of the perovskite. This is confirmed by the orbital analysis of the positive charged states of the n-DMBI-H@Perovskite and the (n-$DMBI^+$ + H^-)@Perovskite systems, see Figure 2c, 2d. As expected, in both cases a clear localization of the hole on the n-DMBI-H molecule and the H ion is observed, respectively. DFT calculations show that the positive (n-$DMBI^+$ + $H^\bullet$)@Perovskite system is slightly less stable than the undissociated positive molecule $(n\text{-}DMBI\text{-}H)^+$@Perovskite by 0.21 eV (see Reaction 2), indicating that in presence of extra holes, i.e., in p-doped substrates, the dissociation of the molecule with hole localization on the H is competitive with the hole localization on the undissociated molecule. Despite being slightly energetically unfavorable, molecular dissociation

at the surface should be entropically favored, further assisting the likelihood of such process at high temperature. Hole transfer from the perovskite substrate to the adsorbed molecule in n-DMBI-H@Perovskite and on the H ion in (n-DMBI$^+$ + H$^-$)@Perovskite are thermodynamically favorable by 0.77 and 0.99 eV, respectively. The doping activity is also confirmed by the analysis of the (+/0) thermodynamic ionization levels of the two systems. In both cases, deep (+/0) transitions placed at 0.42 and 0.64 eV above the VBM are reported for the n-DMBI-H molecule and the splitted (n-DMBI$^+$ + H$^-$) system, see Table S4, highlighting that the positive species are stable for Fermi levels close to the VBM, i.e., in the case of p-doped substrate.

The proposed charge transfer pathway is scrutinized by investigating structural changes in n-DMBI-H before and after contact with perovskite films. Proton nuclear magnetic resonance (^{1}H-NMR) signals of n-DMBI-H (Figure S8) show a downfield shift after interacting with perovskite, indicating lower electron density around the analyzed protons compatible with the formation of cationic molecular dopant species (Reactions 1 and 2). The integration of ^{1}H-NMR peaks in Figure S8 (Table S5) further reveals a relative decrease in labile hydrogens after n-DMBI-H contact with perovskite (~0.86 vs ~0.98), supporting the dopant dissociation mechanism shown herein.

Our results demonstrate that dative bonding between surface Sn in perovskite and amino groups in n-DMBI-H, together with C-H bond dissociation in the molecular dopant, mediates doping compensation in Sn-rich perovskites. This unveils important requisites for efficient carrier density tuning via this class of molecular dopants, namely i) the presence of moieties with Lewis base character and ii) adequate energetic alignment with perovskite hosts; as such, analogues that only satisfy the first condition are not expected to modulate perovskite electronic properties effectively (Figure S9).

The regions within the film microstructure where n-DMBI-H is located and may interact with perovskite are monitored through various imaging techniques. Top-view scanning electron microscopy (SEM) images of perovskite films (Figure 3a) show pinhole-free morphologies with closely packed, submicron-sized grains (~200-500 nm), and indicate that perovskite topography remains unchanged after n-DMBI-H treatment at concentrations up to 1.12 mM. However, we observe dot-like features on perovskite at high concentrations (11.22 mM); possibly, excess n-DMBI-H forms small aggregates upon the saturation of surface Sn sites via dative bonding. To prove homogeneous molecular dopant distribution at the surface, we analyze control and n-DMBI-H-treated perovskite films (0 vs 1.12 mM, respectively) via hyperspectral photoluminescence (PL) imaging (Figure 3b). We note that n-DMBI-H leads to PL quenching in perovskite (Figure S10 and Table S6), which allows mapping of the molecular dopant location on films. In Figure 3b, PL intensity in the n-DMBI-H-treated sample decreases evenly throughout the film microstructure relative to the control sample, corroborating that the molecular dopant is dispersed homogeneously. Slight PL variations within each sample may originate from grain heterogeneity caused by local lattice strain.[34] We further confirm full coverage by the molecular dopant via time-of-flight secondary ion mass spectrometry (ToF-SIMS) surface analysis (Figure S11), which shows a homogeneous distribution of diagnostic ion markers for n-DMBI-H (linear combination of the $C_5H_6N^+$ and $C_{17}H_{20}N_3^+$ ion intensities) on perovskite films.

Possible n-DMBI-H diffusion into $MASn_{0.75}Pb_{0.25}I_3$ films is explored via ToF-SIMS depth profiling (Figure 3c, 1.12 mM; further analysis at higher concentration and imaging of sample interfaces shown in Figures S12 and S13, respectively). The intensity of ions characteristic of perovskite (i.e., MA^+, Sn^+, Pb^+) remains constant and only drops once the indium tin oxide (ITO) substrate is reached (as noted by a concurrent increase in In^+ intensity). In contrast, the n-DMBI-

H ion marker trace reveals a progressive decrease as deeper sample regions are reached, indicating the infiltration of n-DMBI-H into the perovskite layer (most likely via grain boundaries).[35] To visualize the localization of species in the sample and verify that n-DMBI-H penetration into perovskite occurs consistently throughout the film, we employ a ToF-SIMS 3D rendering of secondary ions of interest (3D secondary ion images; Figure 3c). We detect three well-defined sample regions, i.e., a molecular dopant top layer that diffuses into the perovskite film (n-DMBI-H signal, $C_{17}H_{20}N_3^+$), a compact perovskite film (MA^+, Sn^+ and Pb^+ signals) and the ITO bottom layer (In^+ signal). The overlay of n-DMBI-H, Sn^+ and In^+ signals clearly shows that a molecular dopant concentration gradient exists in all scanned regions of the perovskite film. ToF-SIMS analysis of wedge-shaped cross-sections in Figure S13 further confirms a uniform lateral distribution of the dopant in the perovskite film and demonstrates the absence of the $C_{17}H_{20}N_3^+$ ion in control samples. Altogether, the 2D and 3D chemical imaging techniques applied here suggest that n-DMBI-H resides both at the top film surface and within grain boundaries, yielding high contact area between the molecular dopant and perovskite.

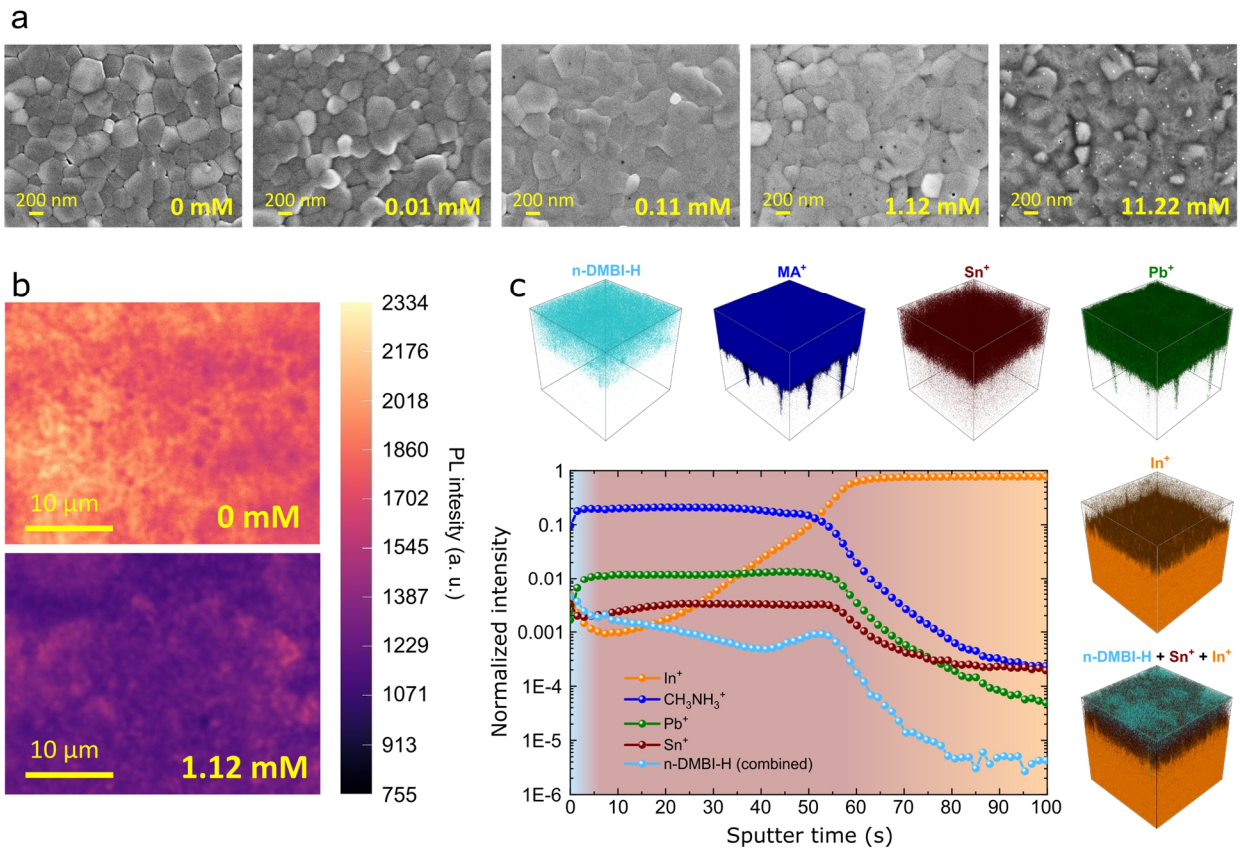

Figure 3. a. Top-view SEM images of n-DMBI-H-treated $MASn_{0.75}Pb_{0.25}I_3$ films at varying molecular dopant concentrations. **b.** Hyperspectral PL imaging of control (0 mM) and n-DMBI-H-treated perovskite films (1.12 mM). **c.** ToF-SIMS depth profiles of perovskite films treated with an n-DMBI-H solution (1.12 mM) and corresponding 3D secondary ion images reconstructed from 100 surface analyses taken at intervals of ~4 µm (field of view: 50µm×50µm).

We assess perovskite doping compensation by exploring the electronic and charge transport properties of n-DMBI-H-treated $MASn_{0.75}Pb_{0.25}I_3$ thin films. As shown in Figure 4a, the mean electrical conductivity (σ) of control perovskite samples (0 mM n-DMBI-H) is ~1.18 $S \cdot cm^{-1}$, in agreement with previous work.[36] Upon increasing n-DMBI-H concentration, σ undergoes a total ~5-fold decrease to ~0.22 $S \cdot cm^{-1}$ (1.12 mM n-DMBI-H). To clarify the trend in σ, we analyze the effect of n-DMBI-H on the majority carrier density (hole density: [p]) and hole mobility (μ_h) of

perovskite films via Hall effect measurements (Figures 4b and 4d). Firstly, Figure 4b shows that the addition of the molecular dopant leads to a reduction in [p]; ranging nearly one order of magnitude from ~$5 \cdot 10^{18}$ cm^{-3} in control samples to ~$7 \cdot 10^{17}$ cm^{-3} in n-DMBI-H-treated films (1.12 mM). We attribute the decrease in [p] to electron transfer from n-DMBI-H to perovskite and therefore the compensation of free holes in perovskite, in good agreement with the mechanistic insights shown above. It must be noted that [p] does not change significantly for concentrations higher than 1.12 mM (11.22 and 67.3 mM; Figure S14). This may arise from minimal dopant-to-perovskite electron transfer upon the saturation of Sn sites with n-DMBI-H, although a strong counteraction effect from p-type Sn^{2+} vacancies in perovskite cannot be ruled out. This strategy is therefore suited for fine-tuning carrier density, rather than to induce a shift to n-type behavior. Future approaches that targets hosts with higher surface area (e.g., low-dimensional perovskites) or introduce specific growth conditions to lessen the impact of intrinsic defects might broaden the range of control over carrier density. Further evidence of doping compensation is obtained via Seebeck coefficient (S) measurements (Figure 4c). Given the inverse proportionality between S and [p] (i.e., $S \propto m^*/[p]^{2/3}$, where m^* represents hole effective mass), we rationalize the increase in S from ~138 $\mu V \cdot K^{-1}$ to ~162 $\mu V \cdot K^{-1}$ (0 mM and 1.12 mM n-DMBI-H, respectively) as a net drop of [p] in the perovskite. Secondly, we analyze μ_h of n-DMBI-H-treated perovskite films in Figure 4d. Control samples exhibit a mean μ_h of ~1.6 $cm^2 \cdot V^{-1} \cdot s^{-1}$ that only drops slightly to ~1.2 $cm^2 \cdot V^{-1} \cdot s^{-1}$ upon 0.01 mM n-DMBI-H treatment, staying this value almost constant at higher molecular dopant concentrations (up to 11.22 mM). We attribute the small loss in μ_h to charge carrier scattering by molecular dopants at grain boundaries. This effect only has a major impact at much higher n-DMBI-H concentrations (i.e., 67.3 mM; Figure S14). We therefore conclude that

the decrease in σ of perovskite films (Figure 4a) is primarily mediated by the compensation of [p] via n-DMBI-H, playing μ_h a minor role due to its relative invariability ($\sigma \propto [p] \cdot \mu_h$).

Further proof of n-DMBI-H-mediated doping compensation is obtained via Kelvin probe (KP) measurements of perovskite films (Figure 4e). Work functions become shallower as n-DMBI-H concentration increases, indicating a weaker p-type character in perovskite as per the trend previously observed for [p] (Figure 4b). The changes in work function registered with the KP are consistent with Ultraviolet Photoelectron Spectroscopy (UPS) measurements (Figure S15; ~0.1 eV difference from 0 mM to 0.01 mM n-DMBI-H in both methods). However, we note that the presence of a molecular dopant overlayer atop perovskite surfaces at high n-DMBI-H concentrations may contribute to the large work function shifts obtained via KP. From the band diagrams in Figure 4f (constructed from optical bandgap and photoelectron spectroscopy measurements; Figure S16), VBMs of perovskite rise upon molecular dopant treatment. This suggests a decrease in ionization energy due to a band filling effect, where electrons donated from the dopant fill the empty states in the valence band and make the highest occupied energy levels shallower.[13,37] Concurrently, optical bandgaps become narrower (from ~1.23 eV to ~1.20 eV in control and 11.22 mM n-DMBI-H-treated samples, respectively), as typically shown in Sn-based perovskite systems upon doping compensation.[13,23]

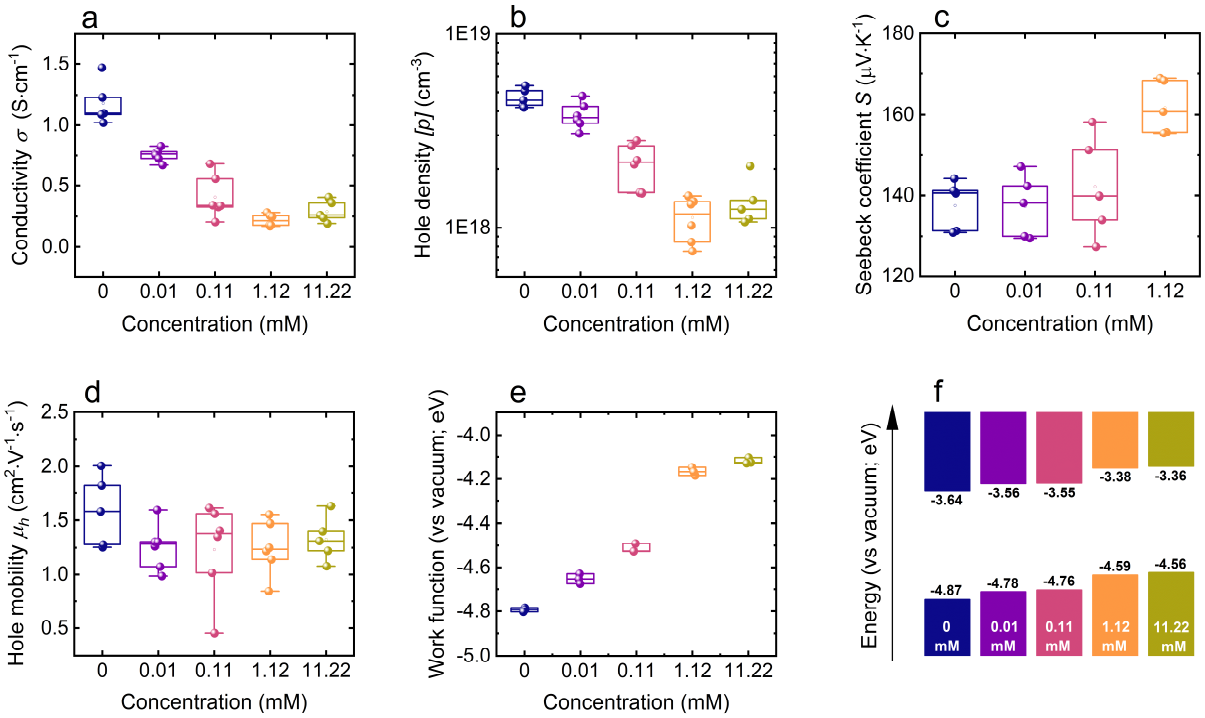

Figure 4. a. Electrical conductivity (σ), **b.** free hole density ([p]), **c.** Seebeck coefficient (S), **d.** Hole mobility (μ_h), **e.** work functions (vs vacuum) and **f.** band edge energies (vs vacuum) of n-DMBI-H-treated $MASn_{0.75}Pb_{0.25}I_3$ thin films.

We have shown that n-DMBI-H modulates carrier density in perovskite through a dissociative adsorption mechanism. To investigate the potential of this avenue in optoelectronics, we apply n-DMBI-H treatments on p-i-n $MASn_{0.75}Pb_{0.25}I_3$ solar cells (architecture: ITO/PEDOT:PSS/Perovskite/PCBM/BCP/Ag). Photovoltaic parameters of our devices and external quantum efficiency (EQE) spectra of champion cells are provided in Figure S17/Table S7 and Figure S18, respectively. Current density-voltage (J-V) curves in Figure 5a clearly show a solar cell performance increase upon molecular dopant treatment, with power conversion efficiencies (PCE) soaring from 3.16% (0 mM n-DMBI-H) to 7.15% (11.22 mM n-DMBI-H). We emphasize that these results are accomplished in absence of any additives (e.g., SnF_2, reducing agents) or compositional engineering (e.g., 2D phases)[38] to isolate the contribution from n-DMBI-

H, reaching a champion PCE comparable to previous examples based on similar perovskite compositions (i.e., MA-based and Sn-rich/Sn-only absorbers).[39–42] Specifically, we observe higher short-circuit current density (J_{sc}; 25.23 mA·cm^{-2} > 15.91 mA·cm^{-2}) and open circuit voltage (V_{oc}; 0.51 V > 0.35 V); we ascribe the decrease in fill factor (FF) at higher n-DMBI-H concentrations (Figure S17) to excess molecular dopant build-up at the perovskite/PCBM interface (Figure 2c). We identify two main routes where mitigating p-type self-doping in perovskite benefits the device performance. Firstly, lowering [p] in Sn-based perovskites (see Figure 4b) is known to enhance their optoelectronic properties[13] and reduce carrier losses in solar cells.[43] In line with this, dark J-V curves in Figure S19 show lower leakage current after n-DMBI-H treatment and suggest lower recombination and enhanced carrier collection consistent with the increase in J_{sc} and V_{oc}.[44] Secondly, n-DMBI-H post-processing enhances the quality of the perovskite/PCBM interface. Time-resolved and steady-state PL in Figure 5b show a stronger PL quenching in perovskite/PCBM bilayers in the presence of molecular dopant (average lifetime, τ_{av}: 5.50 ns > 2.99 ns), implying higher contact selectivity and reduced interfacial recombination.[45] We note that the PL intensity and lifetime of these films is shorter vs pristine perovskite (τ_{av} = 7.40 ns), as expected after adding the PCBM electron transport layer (see Table S6 for fitting parameters). Further information on the link between n-DMBI-H and carrier recombination is provided in Supplementary Note 3. We conclude that managing carrier tuning via n-DMBI-H provides a viable path towards the optimization of Sn-rich perovskite solar cells, suppressing charge losses arising from self-doping and improving interfacial quality between perovskite and PCBM (schematically shown in Figure 5c).

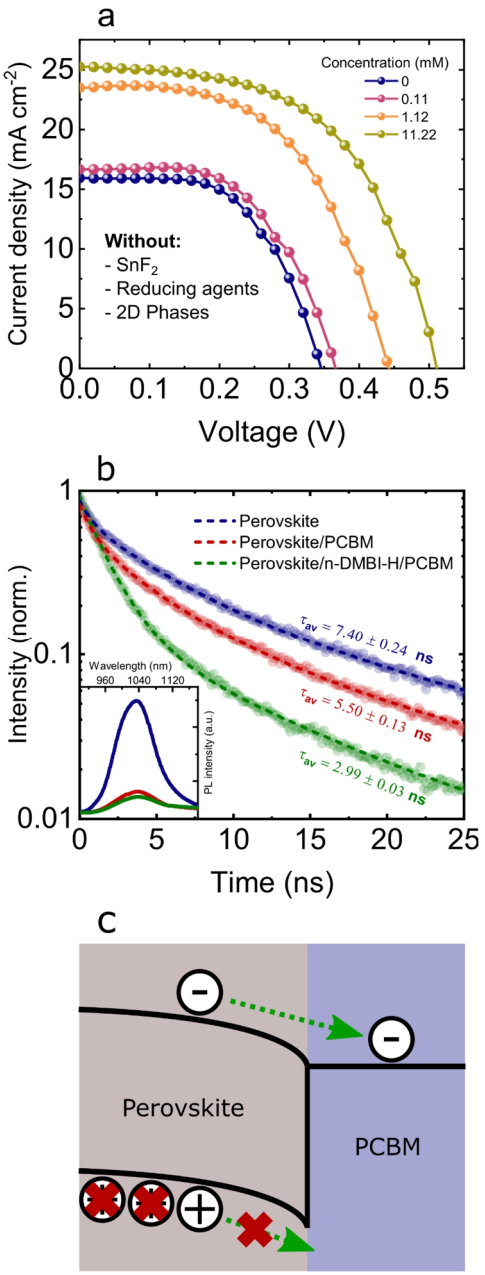

Figure 5. a. *J-V* curves of champion Sn-rich, additive-free perovskite solar cells treated with varying concentrations of n-DMBI-H. **b.** Time-resolved PL decays of control perovskite films and perovskite/PCBM samples with/without n-DMBI-H treatment (1.12 mM). Inset: steady-state PL spectra of samples in the main figure. **c.** Schematic representing n-DMBI-H doping compensation on perovskite solar cells leading to i) reduced free hole density and carrier losses and ii) improved perovskite/PCBM contact quality and selectivity.

In summary, we demonstrated that dissociative bonding between n-type molecular dopant n-DMBI-H and p-type $MASn_{0.75}Pb_{0.25}I_3$ is an essential step to enable carrier tuning in perovskite. Critically, we found perovskite-dopant interactions between amino moieties in n-DMBI-H and Sn atoms in perovskite surface to be key in facilitating charge transfer via perovskite hole trapping at adsorbed dissociated hydride species. Via this mechanism, n-DMBI-H can reduce free hole density by nearly an order of magnitude with minimal impact on carrier mobility, being film surfaces and grain boundaries the targeted sites. We exploited this carrier density tuning route in Sn-rich, additive-free $MASn_{0.75}Pb_{0.25}I_3$ p-i-n solar cells, obtaining improved photovoltaic efficiencies arising from i) reduced self-doping-related carrier losses and ii) higher perovskite/PCBM contact selectivity. The greater fundamental understanding of the underlying doping mechanisms provided herein will enable valuable molecular doping strategies for future perovskite optoelectronics and beyond.

ASSOCIATED CONTENT

Supporting information

Experimental Section; Supplementary Notes and Tables; XRD patterns of perovskite films; optical and electrical stability of perovskite films upon air exposure; peak fitting details of XPS data and Pb *4f* and I *3d* XPS analysis of perovskite films; configuration-dependent adsorption energy of n-DMBI-H onto perovskite; pDOS of pristine perovskite and various host-dopant configurations; thermodynamics of proposed doping compensation pathways; (+/0) transition levels for various host-dopant configurations; ^{1}H-NMR characterization of n-DMBI-H; Hall effect measurements of trimethylamine-treated perovskite films; steady-state and time-resolved perovskite PL and decay fitting details; surface, depth-profile, 3D and wedge-shaped cross-section ToF-SIMS

characterization of perovskite films; additional Hall effect measurements of perovskite films; UPS data of perovskite films, Tauc plots and photoelectron spectroscopy data of perovskite films; photovoltaic parameter statistics of perovskite solar cells; EQE spectra and dark *J-V* curves of champion solar cells (PDF).

AUTHOR INFORMATION

Corresponding authors

Daniele Meggiolaro - Computational Laboratory for Hybrid/Organic Photovoltaics (CLHYO), Istituto CNR di Scienze e Tecnologie Chimiche "'Giulio Natta"' (CNR-SCITEC), Via Elce di Sotto 8, 06123 Perugia, Italy. Email address: daniele.meggiolaro@cnr.it https://orcid.org/0000-0001-9717-133X

Derya Baran - King Abdullah University of Science and Technology (KAUST), Physical Science and Engineering Division (PSE), KAUST Solar Center (KSC), Thuwal, 23955-6900, Saudi Arabia. Email address: derya.baran@kaust.edu.sa https://orcid.org/0000-0003-2196-8187

Authors

Luis Lanzetta - King Abdullah University of Science and Technology (KAUST), Physical Science and Engineering Division (PSE), KAUST Solar Center (KSC), Thuwal, 23955-6900, Saudi Arabia. https://orcid.org/0000-0001-5591-1010

Luca Gregori - Computational Laboratory for Hybrid/Organic Photovoltaics (CLHYO), Istituto CNR di Scienze e Tecnologie Chimiche "'Giulio Natta"' (CNR-SCITEC), Via Elce di Sotto 8, 06123 Perugia, Italy; Department of Chemistry, Biology and Biotechnology, University of Perugia, Via Elce di Sotto 8, 06123, Perugia, Italy. https://orcid.org/0000-0002-0023-8313

Luis Huerta Hernandez - King Abdullah University of Science and Technology (KAUST), Physical Science and Engineering Division (PSE), KAUST Solar Center (KSC), Thuwal, 23955-6900, Saudi Arabia. https://orcid.org/0000-0003-3804-3180

Anirudh Sharma - King Abdullah University of Science and Technology (KAUST), Physical Science and Engineering Division (PSE), KAUST Solar Center (KSC), Thuwal, 23955-6900, Saudi Arabia. https://orcid.org/0000-0003-4841-0108

Stefanie Kern - Advanced Materials & Healthcare Technologies, School of Pharmacy, University of Nottingham, Nottingham, NG7 2RD, UK.

Anna M. Kotowska - Advanced Materials & Healthcare Technologies, School of Pharmacy, University of Nottingham, Nottingham, NG7 2RD, UK. https://orcid.org/0000-0002-4239-1535

Abdul-Hamid Emwas - King Abdullah University of Science and Technology (KAUST), Core Labs, Thuwal 23955-6900, Saudi Arabia.

Luis Gutiérrez-Arzaluz - King Abdullah University of Science and Technology (KAUST), Physical Science and Engineering Division (PSE), Advanced Membranes and Porous Materials and Catalysis Center, Thuwal 23955, Saudi Arabia. https://orcid.org/0000-0001-8971-9377

David J. Scurr – Advanced Materials & Healthcare Technologies, School of Pharmacy, University of Nottingham, Nottingham, NG7 2RD, UK. https://orcid.org/0000-0003-0859-3886

Matthew Piggott – Advanced Materials & Healthcare Technologies, School of Pharmacy, University of Nottingham, Nottingham, NG7 2RD, UK.

Md Azimul Haque - King Abdullah University of Science and Technology (KAUST), Physical Science and Engineering Division (PSE), KAUST Solar Center (KSC), Thuwal, 23955-6900, Saudi Arabia. https://orcid.org/0000-0003-3528-0674

Filippo De Angelis - Computational Laboratory for Hybrid/Organic Photovoltaics (CLHYO), Istituto CNR di Scienze e Tecnologie Chimiche "'Giulio Natta"' (CNR-SCITEC), Via Elce di Sotto 8, 06123 Perugia, Italy; Department of Chemistry, Biology and Biotechnology, University of Perugia, Via Elce di Sotto 8, 06123, Perugia, Italy; Department of Mechanical Engineering, College of Engineering, Prince Mohammad Bin Fahd University, P.O. Box 1664, Al Khobar, 31952, Saudi Arabia; SKKU Institute of Energy Science and Technology (SIEST) Sungkyunkwan University, Suwon, Korea 440-746. https://orcid.org/0000-0003-3833-1975

Twitter Handles

@LanzettaLuis, @DeryaBaranB, @KAUST_OMEGALab, @KAUST_Solar

Notes

The authors declare no competing financial interest.

ACKNOWLEDGMENT

L.L., S.K. and M.P. thank financial support from NanoCAT Funding Scheme (EPSRC Institutional Award, University of Nottingham). D.J.S. acknowledges the financial support of this work by the Engineering and Physical Sciences Research Council (EPSRC; grant code: EP/P029868/1). A.S. greatly acknowledges the support from King Abdullah University of Science and Technology (KAUST) Office of Sponsored Research (OSR) under Award number: OSR-2019-CARF/CCF-3079. This work was supported by the King Abdullah University of Science and Technology (KAUST) Competitive Research Grants under Award number: ORA-CRG10-2021-4668.

REFERENCES

(1) Stoumpos, C. C.; Malliakas, C. D.; Kanatzidis, M. G. Semiconducting Tin and Lead Iodide Perovskites with Organic Cations: Phase Transitions, High Mobilities, and Near-Infrared Photoluminescent Properties. *Inorg. Chem.* **2013**, *52*, 9019–9038.

(2) Meggiolaro, D.; Mosconi, E.; De Angelis, F. Modeling the Interaction of Molecular Iodine with $MAPbI_3$: A Probe of Lead-Halide Perovskites Defect Chemistry. *ACS Energy Lett.* **2018**, *3*, 447–451.

(3) Min, H.; Lee, D. Y.; Kim, J.; Kim, G.; Lee, K. S.; Kim, J.; Paik, M. J.; Kim, Y. K.; Kim, K.

S.; Kim, M. G.; Shin, T. J.; Il Seok, S. Perovskite Solar Cells with Atomically Coherent Interlayers on SnO_2 Electrodes. *Nature* **2021**, *598*, 444–450.

(4) Euvrard, J.; Yan, Y.; Mitzi, D. B. Electrical Doping in Halide Perovskites. *Nat. Rev. Mater.* **2021**, *6*, 531–549.

(5) Haque, M. A.; Rosas Villalva, D.; Hernandez, L. H.; Tounesi, R.; Jang, S.; Baran, D. Role of Dopants in Organic and Halide Perovskite Energy Conversion Devices. *Chem. Mater.* **2021**, *33*, 8147–8172.

(6) Wu, W.; Wang, Q.; Fang, Y.; Shao, Y.; Tang, S.; Deng, Y.; Lu, H.; Liu, Y.; Li, T.; Yang, Z.; Gruverman, A.; Huang, J. Molecular Doping Enabled Scalable Blading of Efficient Hole-Transport-Layer-Free Perovskite Solar Cells. *Nat. Commun.* **2018**, *9*, 1625.

(7) Liu, A.; Zhu, H.; Reo, Y.; Kim, M.-G.; Chu, H. Y.; Lim, J. H.; Kim, H.-J.; Ning, W.; Bai, S.; Noh, Y.-Y. Modulation of Vacancy-Ordered Double Perovskite Cs_2SnI_6 for Air-Stable Thin-Film Transistors. *Cell Reports Phys. Sci.* **2022**, *3*, 100812.

(8) Reo, Y.; Zhu, H.; Liu, A.; Noh, Y. Y. Molecular Doping Enabling Mobility Boosting of 2D Sn^{2+}-Based Perovskites. *Adv. Funct. Mater.* **2022**, 2204870.

(9) Shyamal, S.; Dutta, S. K.; Pradhan, N. Doping Iron in $CsPbBr_3$ Perovskite Nanocrystals for Efficient and Product Selective CO2 Reduction. *J. Phys. Chem. Lett.* **2019**, *10*, 7965–7969.

(10) Phung, N.; Félix, R.; Meggiolaro, D.; Al-Ashouri, A.; Sousa E Silva, G.; Hartmann, C.; Hidalgo, J.; Köbler, H.; Mosconi, E.; Lai, B.; Gunder, R.; Li, M.; Wang, K. L.; Wang, Z. K.; Nie, K.; Handick, E.; Wilks, R. G.; Marquez, J. A.; Rech, B.; Unold, T.; Correa-Baena, J. P.; Albrecht, S.; De Angelis, F.; Bär, M.; Abate, A. The Doping Mechanism of Halide Perovskite Unveiled by Alkaline Earth Metals. *J. Am. Chem. Soc.* **2020**, *142*, 2364–2374.

(11) Kumar, M. H.; Dharani, S.; Leong, W. L.; Boix, P. P.; Prabhakar, R. R.; Baikie, T.; Shi, C.; Ding, H.; Ramesh, R.; Asta, M.; Graetzel, M.; Mhaisalkar, S. G.; Mathews, N. Lead-Free Halide Perovskite Solar Cells with High Photocurrents Realized Through Vacancy Modulation. *Adv. Mater.* **2014**, *26*, 7122–7127.

(12) Ulatowski, A. M.; Wright, A. D.; Wenger, B.; Buizza, L. R. V.; Motti, S. G.; Eggimann, H. J.; Savill, K. J.; Borchert, J.; Snaith, H. J.; Johnston, M. B.; Herz, L. M. Charge-Carrier Trapping Dynamics in Bismuth-Doped Thin Films of $MAPbBr_3$ Perovskite. *J. Phys. Chem. Lett.* **2020**, *11*, 3681–3688.

(13) Savill, K. J.; Ulatowski, A. M.; Farrar, M. D.; Johnston, M. B.; Snaith, H. J.; Herz, L. M. Impact of Tin Fluoride Additive on the Properties of Mixed Tin-Lead Iodide Perovskite Semiconductors. *Adv. Funct. Mater.* **2020**, *30*, 2005594.

(14) Noel, N. K.; Habisreutinger, S. N.; Pellaroque, A.; Pulvirenti, F.; Wenger, B.; Zhang, F.; Lin, Y. H.; Reid, O. G.; Leisen, J.; Zhang, Y.; Barlow, S.; Marder, S. R.; Kahn, A.; Snaith, H. J.; Arnold, C. B.; Rand, B. P. Interfacial Charge-Transfer Doping of Metal Halide Perovskites for High Performance Photovoltaics. *Energy Environ. Sci.* **2019**, *12*, 3063–3073.

(15) Jiang, Q.; Ni, Z.; Xu, G.; Lin, Y.; Rudd, P. N.; Xue, R.; Li, Y.; Li, Y.; Gao, Y.; Huang, J. Interfacial Molecular Doping of Metal Halide Perovskites for Highly Efficient Solar Cells. *Adv. Mater.* **2020**, *32*, 2001581.

(16) Euvrard, J.; Gunawan, O.; Zhong, X.; Harvey, S. P.; Kahn, A.; Mitzi, D. B. P-Type Molecular Doping by Charge Transfer in Halide Perovskite. *Mater. Adv.* **2021**, *2*, 2956–2965.

(17) Scaccabarozzi, A. D.; Basu, A.; Aniés, F.; Liu, J.; Zapata-Arteaga, O.; Warren, R.; Firdaus, Y.; Nugraha, M. I.; Lin, Y.; Campoy-Quiles, M.; Koch, N.; Müller, C.; Tsetseris, L.; Heeney, M.; Anthopoulos, T. D. Doping Approaches for Organic Semiconductors. *Chem. Rev.* **2022**, *122*, 4420–4492.

(18) Paterson, A. F.; Li, R.; Markina, A.; Tsetseris, L.; Macphee, S.; Faber, H.; Emwas, A. H.; Panidi, J.; Bristow, H.; Wadsworth, A.; Baran, D.; Andrienko, D.; Heeney, M.; McCulloch, I.; Anthopoulos, T. D. N-Doping Improves Charge Transport and Morphology in the Organic Non-Fullerene Acceptor O-IDTBR. *J. Mater. Chem. C* **2021**, *9*, 4486–4495.

(19) Zeng, Y.; Zheng, W.; Guo, Y.; Han, G.; Yi, Y. Doping Mechanisms of N-DMBI-H for

Organic Thermoelectrics: Hydrogen Removal vs. Hydride Transfer. *J. Mater. Chem. A* **2020**, *8*, 8323–8328.

(20) Chen, H.; Zhan, Y.; Xu, G.; Chen, W.; Wang, S.; Zhang, M.; Li, Y.; Li, Y. Organic N-Type Molecule: Managing the Electronic States of Bulk Perovskite for High-Performance Photovoltaics. *Adv. Funct. Mater.* **2020**, *30*, 2001788.

(21) Huang, Z.; Wei, M.; Proppe, A. H.; Chen, H.; Chen, B.; Hou, Y.; Ning, Z.; Sargent, E. Band Engineering via Gradient Molecular Dopants for CsFA Perovskite Solar Cells. *Adv. Funct. Mater.* **2021**, *31*, 2010572.

(22) Lanzetta, L.; Aristidou, N.; Haque, S. A. Stability of Lead and Tin Halide Perovskites: The Link between Defects and Degradation. *J. Phys. Chem. Lett.* **2020**, *11*, 574–585.

(23) Milot, R. L.; Klug, M. T.; Davies, C. L.; Wang, Z.; Kraus, H.; Snaith, H. J.; Johnston, M. B.; Herz, L. M. The Effects of Doping Density and Temperature on the Optoelectronic Properties of Formamidinium Tin Triiodide Thin Films. *Adv. Mater.* **2018**, *30*, 1804506.

(24) Yuan, F.; Zheng, X.; Johnston, A.; Wang, Y.; Zhou, C.; Dong, Y.; Chen, B.; Chen, H.; Fan, J. Z.; Sharma, G.; Li, P.; Gao, Y.; Voznyy, O.; Kung, H.; Lu, Z.; Bakr, O. M.; Sargent, E. H. Color-Pure Red Light-Emitting Diodes Based on Two-Dimensional Lead-Free Perovskites. *Sci. Adv.* **2020**, *6*, eabb0253.

(25) Liu, A.; Zhu, H.; Bai, S.; Reo, Y.; Zou, T.; Kim, M. G.; Noh, Y. Y. High-Performance Inorganic Metal Halide Perovskite Transistors. *Nat. Electron.* **2022**, *5*, 78–83.

(26) Zhang, T.; Li, H.; Ban, H.; Sun, Q.; Shen, Y.; Wang, M. Efficient $CsSnI_3$-Based Inorganic Perovskite Solar Cells Based on a Mesoscopic Metal Oxide Framework via Incorporating a Donor Element. *J. Mater. Chem. A* **2020**, *8*, 4118–4124.

(27) Leijtens, T.; Prasanna, R.; Gold-Parker, A.; Toney, M. F.; McGehee, M. D. Mechanism of Tin Oxidation and Stabilization by Lead Substitution in Tin Halide Perovskites. *ACS Energy Lett.* **2017**, *2*, 2159–2165.

(28) Mundt, L. E.; Tong, J.; Palmstrom, A. F.; Dun, S. P.; Zhu, K.; Berry, J. J.; Schelhas, L. T.;

Ratcli, E. L. Surface-Activated Corrosion in Tin − Lead Halide Perovskite Solar Cells. *ACS Energy Lett.* **2020**, *5*, 3344–3351.

(29) Westbrook, R. J. E.; Macdonald, T. J.; Xu, W.; Lanzetta, L.; Marin-Beloqui, J. M.; Clarke, T. M.; Haque, S. A. Lewis Base Passivation Mediates Charge Transfer at Perovskite Heterojunctions. *J. Am. Chem. Soc.* **2021**, *143*, 12230–12243.

(30) Wang, X. D.; Huang, Y. H.; Liao, J. F.; Wei, Z. F.; Li, W. G.; Xu, Y. F.; Chen, H. Y.; Kuang, D. Bin. Surface Passivated Halide Perovskite Single-Crystal for Efficient Photoelectrochemical Synthesis of Dimethoxydihydrofuran. *Nat. Commun.* **2021**, *12*, 1202.

(31) Reiser, P.; Benneckendorf, F. S.; Barf, M. M.; Müller, L.; Bäuerle, R.; Hillebrandt, S.; Beck, S.; Lovrincic, R.; Mankel, E.; Freudenberg, J.; Jänsch, D.; Kowalsky, W.; Pucci, A.; Jaegermann, W.; Bunz, U. H. F.; Müllen, K. N-Type Doping of Organic Semiconductors: Immobilization via Covalent Anchoring. *Chem. Mater.* **2019**, *31*, 4213–4221.

(32) Lu, Y.; Yu, Z. Di; Liu, Y.; Ding, Y. F.; Yang, C. Y.; Yao, Z. F.; Wang, Z. Y.; You, H. Y.; Cheng, X. F.; Tang, B.; Wang, J. Y.; Pei, J. The Critical Role of Dopant Cations in Electrical Conductivity and Thermoelectric Performance of N-Doped Polymers. *J. Am. Chem. Soc.* **2020**, *142*, 15340–15348.

(33) Bardagot, O.; Aumaître, C.; Monmagnon, A.; Pécaut, J.; Bayle, P. A.; Demadrille, R. Revisiting Doping Mechanisms of N-Type Organic Materials with N-DMBI for Thermoelectric Applications: Photo-Activation, Thermal Activation, and Air Stability. *Appl. Phys. Lett.* **2021**, *118*, 203904.

(34) Jones, T. W.; Osherov, A.; Alsari, M.; Sponseller, M.; Duck, B. C.; Jung, Y. K.; Settens, C.; Niroui, F.; Brenes, R.; Stan, C. V.; Li, Y.; Abdi-Jalebi, M.; Tamura, N.; MacDonald, J. E.; Burghammer, M.; Friend, R. H.; Bulović, V.; Walsh, A.; Wilson, G. J.; Lilliu, S.; Stranks, S. D. Lattice Strain Causes Non-Radiative Losses in Halide Perovskites. *Energy Environ. Sci.* **2019**, *12*, 596–606.

(35) Yang, B.; Dyck, O.; Poplawsky, J.; Keum, J.; Puretzky, A.; Das, S.; Ivanov, I.; Rouleau, C.; Duscher, G.; Geohegan, D.; Xiao, K. Perovskite Solar Cells with Near 100% Internal

Quantum Efficiency Based on Large Single Crystalline Grains and Vertical Bulk Heterojunctions. *J. Am. Chem. Soc.* **2015**, *137*, 9210–9213.

(36) Haque, M. A.; Hernandez, L. H.; Davaasuren, B.; Villalva, D. R.; Troughton, J.; Baran, D. Tuning the Thermoelectric Performance of Hybrid Tin Perovskites by Air Treatment. *Adv. Energy Sustain. Res.* **2020**, *1*, 2000033.

(37) Perry, E. E.; Labram, J. G.; Venkatesan, N. R.; Nakayama, H.; Chabinyc, M. L. N-Type Surface Doping of $MAPbI_3$ via Charge Transfer from Small Molecules. *Adv. Electron. Mater.* **2018**, *4*, 1800087.

(38) Yu, D.; Wei, Q.; Li, H.; Xie, J.; Jiang, X.; Pan, T.; Wang, H.; Pan, M.; Zhou, W.; Liu, W.; Chow, P. C. Y.; Ning, Z. Quasi-2D Bilayer Surface Passivation for High Efficiency Narrow Bandgap Perovskite Solar Cells. *Angew. Chem. Int. Ed.* **2022**, *61*, e202202346.

(39) Zhao, B.; Abdi-Jalebi, M.; Tabachnyk, M.; Glass, H.; Kamboj, V. S.; Nie, W.; Pearson, A. J.; Puttisong, Y.; Gödel, K. C.; Beere, H. E.; Ritchie, D. A.; Mohite, A. D.; Dutton, S. E.; Friend, R. H.; Sadhanala, A. High Open-Circuit Voltages in Tin-Rich Low-Bandgap Perovskite-Based Planar Heterojunction Photovoltaics. *Adv. Mater.* **2017**, *29*, 1604744.

(40) Tavakoli, M. M.; Zakeeruddin, S. M.; Grätzel, M.; Fan, Z. Large-Grain Tin-Rich Perovskite Films for Efficient Solar Cells via Metal Alloying Technique. *Adv. Mater.* **2018**, *30*, 1705998.

(41) Li, F.; Zhang, C.; Huang, J. H.; Fan, H.; Wang, H.; Wang, P.; Zhan, C.; Liu, C. M.; Li, X.; Yang, L. M.; Song, Y.; Jiang, K. J. A Cation-Exchange Approach for the Fabrication of Efficient Methylammonium Tin Iodide Perovskite Solar Cells. *Angew. Chem. Int. Ed.* **2019**, *58*, 6688–6692.

(42) Wang, P.; Li, F.; Jiang, K. J.; Zhang, Y.; Fan, H.; Zhang, Y.; Miao, Y.; Huang, J. H.; Gao, C.; Zhou, X.; Wang, F.; Yang, L. M.; Zhan, C.; Song, Y. L. Ion Exchange/Insertion Reactions for Fabrication of Efficient Methylammonium Tin Iodide Perovskite Solar Cells. *Adv. Sci.* **2020**, *7*, 1903047.

(43) Lanzetta, L.; Webb, T.; Zibouche, N.; Liang, X.; Ding, D.; Min, G.; Westbrook, R. J. E.;

Gaggio, B.; Macdonald, T. J.; Islam, M. S.; Haque, S. A. Degradation Mechanism of Hybrid Tin-Based Perovskite Solar Cells and the Critical Role of Tin (IV) Iodide. *Nat. Commun.* **2021**, *12*, 2853.

(44) Ke, W.; Stoumpos, C. C.; Spanopoulos, I.; Chen, M.; Wasielewski, M. R.; Kanatzidis, M. G. Diammonium Cations in the FASnI 3 Perovskite Structure Lead to Lower Dark Currents and More E Ffi Cient Solar Cells. *ACS Energy Lett.* **2018**, *3*, 1470–1476.

(45) Macdonald, T. J.; Clancy, A. J.; Xu, W.; Jiang, Z.; Lin, C.-T.; Mohan, L.; Du, T.; Tune, D. D.; Lanzetta, L.; Min, G.; Webb, T.; Ashoka, A.; Pandya, R.; Tileli, V.; McLachlan, M. A.; Durrant, J. R.; Haque, S. A.; Howard, C. A. Phosphorene Nanoribbon-Augmented Optoelectronics for Enhanced Hole Extraction. *J. Am. Chem. Soc.* **2021**, *143*, 21549–21559.